Learning the Inverse Dynamics of Robotic Manipulators in Structured Reproducing Kernel Hilbert Space

Ching-An Cheng, Han-Pang Huang*, *Member, IEEE,* Huan-Kun Hsu, Wei-Zh Lai, Chih-Chun Cheng

***Abstract*—We investigate the modeling of inverse dynamics without prior kinematic information for holonomic rigid-body robots. Despite success in compensating robot dynamics and friction, general inverse dynamics models are nontrivial. Rigid-body models are restrictive or inefficient; learning-based models are generalizable yet require large training data. The structured kernels address the dilemma by embedding the robot dynamics in reproducing kernel Hilbert space. The proposed kernels autonomously converge to rigid-body models but require fewer samples; with a semi-parametric framework that incorporates additional parametric basis for friction, the structured kernels can efficiently model general rigid-body robots. We tested the proposed scheme in simulations and experiments; the models that consider the structure of function space are more accurate.**

***Index Terms*—Inverse Dynamics, Intelligent Robots, Reproducing Kernel Hilbert Space, System Identification.**

I. Introduction

Robots that exploit inverse dynamics as feedforward compensation perform better in tracking and force control [1, 2]. In particular, an inverse model is indispensable for impedance control to perform the desired behavior [3] or for exoskeleton to estimate human intention [4].

On the basis of modeling criteria, we categorize the literatures into the parametric models based on rigid-body assumption and the machine learning models based on approximation theory. Under the assumptions that all links of a robot are rigid and that friction can be disregarded, traditional *rigid-body models* [5-10] are parameterized by *kinematic parameters* and *inertial parameters*, in which kinematic parameters specify Denavit-Hartenberg (DH) model, whereas inertial parameters consist of the inertia matrix as well as the mass and the position of each link's center of mass. In modeling, Newton-Euler method [6] and energy formulation [8], with kinematic parameters pre-calibrated by laser [11] or camera [12], identify the inertial parameters in linear regression, suffering from accumulated kinematic errors; Euler-Lagrange method [13] explores both kinematic and inertial unknowns by linear regression, suffering from the curse of dimensionality in computation due to the lack of kinematic information, especially for robots with large degrees of freedom (DOF). In addition, the dynamics of general closed-loop robots may be difficult to be casted in linear form [14], and none of the rigid-body models above directly considers friction. Therefore, an analytic rigid-body model is suitable, only if unmodeled dynamics exert negligible strength.

Learning-based models have been proposed as alternatives, considering uncertainties due to friction, joint flexibility, and manufacturing errors [15-21]. Dated back to the advent of neural networks and the subsequent kernel methods based on reproducing kernel Hilbert space (RKHS), these flexible learners approximate a system only by inputs and outputs [16, 19, 22, 23], improve the analytic model [24], use the rigid-body model as prior information to boost performance [17, 25].

In this paper, we study the autonomous modeling of inverse dynamics for general holonomic rigid-body robots using *only* system inputs and outputs. Without kinematic information, most rigid-body models fail or become infeasible; although several papers based on rigid-body model [26, 27] addressed this issue by exploiting linear form of Jacobian matrix, an external sensor (e.g. camera) remains necessary. By contrast, learning-based models are natural extensions for this setting but often requires large amount of samples. In particular, the popular radial basis function (rbf) kernels in the form of $k(x_i, x_j) = k(\|x_i - x_j\|)$ often fail to generalize, underestimating the predicted torque. Although identically independently distributed (i.i.d.) sampling stochastically relaxes the requirement, samples fail to meet general applications (with iterative learning control [28] as an exception). The curse of dimensionality in sufficient samples still challenges.

On the basis of our preliminary results [29], we propose a family of finite-dimensional reproducing kernels that embed the structure of rigid-body dynamics—the *structured kernels*. By designing appropriate RKHSs, we can directly model rigid-body dynamics with neither kinematic information nor Euler-Lagrange method. Furthermore, these computationally efficient structured kernels limit the covering number of the hypothesis space: learning automatically, the proposed approach requires fewer samples than general learning-based models, and even uniformly converges to the rigid-body model

C.-A. Cheng, H.-K. Hsu, W.-Z. Lai, and C.-C. Cheng, are with the Department of Mechanical Engineering, National Taiwan University, Taipei, Taiwan, 10617, R.O.C. (C.-A. Cheng: r00522817@ntu.edu.tw)

H.-P. Huang is with the Department of Mechanical Engineering, National Taiwan University, Taipei, Taiwan, 10617, R.O.C. (Corresponding addressee: hanpang@ntu.edu.tw).

with finite samples.

In application, we further adopt it in a semi-parametric framework with parametric functions for friction. Transformed into a multiple kernel fashion, this frameworks can be easily incorporated in any off-shelve, state-of-the-art kernel methods (e.g. regularized least-square, Gaussian process regression, and support vector regression). Finally, in simulations and experiments, we test the generalization performance in prediction and tracking with pre-computed torque control. The results show that the models with structured kernels are more accurate.

The rest of the paper is organized as follows. Section II presents the main results: the structured kernels and the convergence analysis. Section III demonstrates the method by which the semi-parametric framework can be approximated by multiple kernels. The simulations and the experimental results are presented in Sections IV and V and discussed in Section VI. Finally, Section VII concludes the paper.

II. Structured Reproducing Kernel Hilbert Space of Rigid-Body Dynamics

To analyze the RKHS of inverse dynamics, we begin with the notations used throughout the subsequent derivation. For an *N*-DOF robot, $q \in \mathbb{R}^N$ denotes its generalized coordinates, and $x := (q, \dot{q}, \ddot{q}) \in \mathbb{R}^{3N}$ denotes its state vector. We assume that $\|x\|_\infty < \infty$ during the robot's entire operation, and define the compact subset $\mathcal{X}$ as the union of all possible states endowed with probability measure ρ_x. For simplicity, with the abuse of notation, we denote $q \in \mathcal{X}$ as that q belongs to the set of all possible positions, and denote $F \in \mathcal{G}$ as that the column space of F is included in the span of $\{g_n e_n \mid g_n \in \mathcal{G}, n \in \mathbb{N}_N\}$, in which $F \in \mathbb{R}^{N\times M}$ is a matrix function, $\mathcal{G}$ is a scalar function space, and $e_n \in \mathbb{R}^N$ is the *n*th standard basis of $\mathbb{R}^N$.

In modeling, we treat the identification of inverse dynamics of an *N*-DOF robot as *N* independent scalar regression problems, i.e. each joint model is identified independently. Without loss of generality, we assume that the robot is serial and that all joints are rotary, because the proposed scheme can be trivially generalized to robots with prismatic joints or close loop [30].

Our goal is to design a hypothesis space as a subset in $C(\mathcal{X})$ that contains inverse dynamics yet presents low complexity so that a model can effectively generalize without directly confronting the curse of dimensionality. Expressing rigid-body robot dynamics in the Euler-Lagrange equation, we treat the inverse dynamics as the image of the Lagrangian under a linear map and model the RKHS for the Lagrangian. Exploiting this relationship, our result identifies a finite-dimensional RKHS $\mathcal{H}_{pol}$ with hybrid polynomial kernel, in which the uniform convergence to the rigid-body dynamics is possible even under finite observations.

A. Euler-Lagrange Formulation

We begin with analyzing the Euler-Lagrange formulation of robot dynamics [30]. For an *N*-DOF robot, let

$$
\begin{aligned}
T(q,\dot{q}) &= \frac{1}{2}\dot{q}^T M(q)\dot{q} \qquad (1)\\
&= \frac{1}{2}\dot{q}^T \sum_{i=1}^{N}\Big[m_i J_{v_i}(q)^T J_{v_i}(q) + J_{\omega_i}(q)^T R_i(q)\Omega_i R_i(q)^T J_{\omega_i}(q)\Big]\dot{q}
\end{aligned}
$$

$$
U(q) = \sum_{i=1}^{N} -m_i g^T r_{ci}(q) \qquad (2)
$$

be the kinematic energy and the potential energy, respectively, and define the Lagrangian as

$$
L := T - U \ , \qquad (3)
$$

in which m_i is the mass, r_{ci} is the position of the center of mass, Ω_i is the inertia matrix, J_{v_i} is the Jacobian matrix of linear velocity, J_{ω_i} is the Jacobian matrix of angular velocity, R_i is the rotational matrix between the inertial frame to joint frame of link i , g is the gravitational acceleration vector, and $M(q) \in \mathbb{R}^{N\times N}$ is the generalized inertia matrix of the entire robot.

The Euler-Lagrange equation shows that the generalized force is the image of the Lagrangian under a linear map defined by the differential operator:

$$
f_{dyn,n}(x) = (\frac{d}{dt}\frac{\partial}{\partial \dot{q}_n} - \frac{\partial}{\partial q_n})L = \tau_n \ , \qquad (4)
$$

which can be summarized in the form as

$$
f_{dyn}(x) = M(q)\ddot{q} + C(q,\dot{q})\dot{q} + G(q) = \tau \ , \qquad (5)
$$

in which $f_{dyn,n} : \mathbb{R}^{3N} \to \mathbb{R}$ is the inverse dynamics of the *nth* generalized coordinate, q_n is the *n*th generalized coordinate and τ_n is the *n*th generalized force, $M(q) \in \mathbb{R}^{N\times N}$ is the inertia matrix as defined in (1), $C(q,\dot{q}) \in \mathbb{R}^{N\times N}$ is the Coriolis/centrifugal matrix, $G(q) \in \mathbb{R}^N$ is the gravitational term, $f_{dyn} := (f_{dyn,\mathrm{n}})_{n\in\mathbb{N}_N}$ $\tau := (\tau_n)_{n\in\mathbb{N}_N}$, and $\mathbb{N}_N := \{1,...,N\}$. In particular, $f_{dyn,\mathrm{n}} \in C^\infty(\mathcal{X})$, the Banach space of smooth functions.

In the context of robotics, modeling with (4) is referred to as Euler-Lagrange method, in which the unknowns, including both kinematic and dynamic parameters, can be arranged in a linear form. However, its worst-case computational complexity exponentially explodes, if prior information of kinematics is unavailable. Therefore, the exact formulation of (4) for general robots is intricate and computationally intractable even with symbolic mathematics toolbox.

B. Finite Dimensional Reproducing Kernel Hilbert Space of Rigid-Body Dynamics

Let $\mathcal{H}_{pol}$ be the proposed structured RKHS. In the following, we derive its reproducing kernel k_{pol} and show that $\mathcal{H}_{pol}$ is a finite-dimensional space containing (4). First, we analyze the RKHS that contains the Lagrangian. Then we design $\mathcal{H}_{pol}$ by identifying a computationally efficient kernel whose span includes the image of the Lagrangian of arbitrary rigid-body dynamics under the linear map in (4), and incorporate it with a parameter to regulate its complexity.

A RKSH $\mathcal{H}$ [31, 32] is a vector space of continuous functions with the reproducing property

$$f(x) = \langle f, k_x \rangle_{\mathcal{H}},\ \forall f \in \mathcal{H}\ , \tag{6}$$

in which k_x is the corresponding reproducing kernel of $\mathcal{H}$, so the evaluation of a function $f \in \mathcal{H}$ on x is the projection on the kernel vector k_x. Consequently, the learning problem of an unknown function f with finite observations becomes the inference problem with the projection of f on the subspace spanned by the observations, which can be solved by kernel methods.

However, the choice of RKHS is nontrivial and considerably affects the result. Learning in a RKHS of small capacity can enable fast convergence but may introduce bias, whereas learning in a universal and large RKHS is prone to variance. This observation motivates us to identify a RKHS that is large enough to contain (4) yet sufficiently small enough to prevent over-fitting to finite samples. A particularly favorable option is a finite-dimensional space, for which uniform convergence is possible even with finite samples. Furthermore, this RKHS should be endowed with a computationally efficient reproducing kernel function for real-time applicability.

To model the RKHS for the Lagrangian, we first introduce three RKHSs, $\mathcal{H}_{\ddot{q}}$, $\mathcal{H}_{\dot{q}\otimes\dot{q}}$, and $\mathcal{H}_{\psi}$, with the reproducing kernels

$$k_{\ddot{q}}(x_i, x_j) = N^{-1}\langle \ddot{q}_i, \ddot{q}_j \rangle \tag{7}$$

$$k_{\dot{q}\otimes\dot{q}}(x_i, x_j) = N^{-2}\langle \dot{q}_i, \dot{q}_j \rangle^2 \tag{8}$$

$$k_{\psi}(x_i, x_j) = \prod_{n\in\mathbb{N}_N} (\cos(q_i - q_j) + 1)\ . \tag{9}$$

Proposition 1

$k_{\ddot{q}}$, $k_{\dot{q}\otimes\dot{q}}$, k_{ψ} are positive definite kernels.

Proof: The proof for first two kernels is trivial. For k_{ψ}, define a nonlinear map $\psi : \mathcal{X} \to \mathbb{R}^{3^N}$ as

$$x = (q, \dot{q}, \ddot{q}) \to \bigotimes_{n\in\mathbb{N}_N} (\cos q_n, \sin q_n, 1)\ . \tag{10}$$

By the trigonometric identity, $k_{\psi}(x_i, x_j) = \langle \psi(x_j), \psi(x_i) \rangle$. □

$\mathcal{H}_{\ddot{q}}$, $\mathcal{H}_{\dot{q}\otimes\dot{q}}$, and $\mathcal{H}_{\psi}$ are well-defined RKHSs: $\mathcal{H}_{\ddot{q}}$ contains the functions linear in $\ddot{q}$, $\mathcal{H}_{\dot{q}\otimes\dot{q}}$ contains the functions quadratic in $\dot{q}$, and $\mathcal{H}_{\psi}$ contains the functions multi-linear in $\{\cos q_n, \sin q_n, 1\}$ for $n \in \mathbb{N}_N$. In addition, we introduce the normalization factor N^{-1} to control the complexity such that the norm of the kernel functions (7)–(9) is bounded regardless of N given $\|x\|_\infty < \infty$ (The factor N^{-1} can be removed if a constraint $\|x\| < x_{\max}$ is imposed instead of $\|x\|_\infty < x_{\max}$, for some $x_{\max} > 0$. We choose the latter, because it can be more efficiently checked).

With these three elementary RKHSs, we can identify the RKHS for the Lagrangian by identifying the RKHSs for the kinematic energy and potential energy in (1) and (2).

Proposition 2

The kinematic energy and the potential energy of rigid-body dynamics lie in the following RKHSs,

$$T \in \mathcal{H}_{\dot{q}\otimes\dot{q}} \otimes \mathcal{H}_{\psi} \otimes \mathcal{H}_{\psi} =: \mathcal{H}_T\ , \tag{11}$$

$$U \in \mathcal{H}_{\psi} =: \mathcal{H}_U\ . \tag{12}$$

Namely, $L \in \mathcal{H}_T \oplus \mathcal{H}_U$.

Proof: Let a serial robot be indexed in accordance with DH convention, in which frame i-1 is defined with respect to link i, and the two endpoints of link i are joint i and joint i+1. Then the nth column of linear Jacobian J_{v_i} and angular Jacobian J_{ω_i} of frame i can be written as

$$J_{v_i,n} = \begin{cases} \partial r_{ci} / \partial q_n, & \text{if } n \le i \\ 0, & \text{else} \end{cases}, \tag{13}$$

$$J_{\omega_i,n} = \begin{cases} \rho_n z_{n-1}, & \text{if } n \le i \\ 0, & \text{else} \end{cases}, \tag{14}$$

in which ρ_n is 0, if joint n is prismatic, and is 0, if joint n is rotary, r_{ci} is the position of frame i, z_{n-1} is the axis of the nth generalized coordinate, and $n \in \mathbb{N}_N$.

Assume all the joints are rotary (the derivation for prismatic joints is simpler and similar). Because the kinematic energy and the potential energy can be represented in the body frame, to prove Proposition 2, it is sufficient to show that the column space of J_{v_i} and $R_i^T J_{\omega_i}$ in (1) are in $\mathcal{H}_{\psi}$. For linear velocity, $J_{v_i} \in \mathcal{H}_{\psi}$ because $r_{ci} \in \mathcal{H}_{\psi}$ and the linear operator $\partial / \partial q_n$ maps all elements in $\mathcal{H}_{\psi}$ to $\mathcal{H}_{\psi}$; for angular velocity, $J_{\omega_i} \in \mathcal{H}_{\psi}$ because $R_i^T \rho_n z_{n-1} = \rho_n R_{i-1}^{0\ T} R_n^0 e_3 = \rho_n R_n^{i-1} e_3$ and $R_n^{i-1} e_3 \in \mathcal{H}_{\psi}$ ($R_i(q)$ is the rotation from frame i to inertial frame), in which $e_3 \in \mathbb{R}^3$ is the standard basis of z-axis. As for the potential energy, the derivation is similar. Finally, because $L = T - U$, $L \in \mathcal{H}_T \oplus \mathcal{H}_U$. □

Finally, we design RKHS $\mathcal{H}_{pol}$ as a RKHS that contains the image of $\mathcal{H}_T \oplus \mathcal{H}_U$ under the linear map in (4). Because $\mathcal{L} \in \mathcal{H}_T \oplus \mathcal{H}_U$, there exists $f_{dyn} \in \mathcal{H}_{pol}$ for arbitrary rigid-body robots.

Theorem 1

Let $\mathrm{Im}(\mathcal{H}_T \oplus \mathcal{H}_U)_n$ *be the image of* $\mathcal{H}_T \oplus \mathcal{H}_U$ *under the linear map,*

$$T_n := \left(\frac{d}{dt}\frac{\partial}{\partial \dot{q}_n} - \frac{\partial}{\partial q_n}\right),\ n \in \mathbb{N}_N\ . \tag{15}$$

Then $\mathrm{Im}(\mathcal{H}_T \oplus \mathcal{H}_U)_n$ *can be included in the following RKHS*

$$\mathcal{H}_{pol} := (\mathcal{H}_{\ddot{q}} \oplus \mathcal{H}_{\dot{q}\otimes\dot{q}}) \otimes (\mathcal{H}_{\psi} \otimes \mathcal{H}_{\psi}) \oplus \mathcal{H}_{\psi} \setminus \mathcal{H}_1\ , \tag{16}$$

for all $n \in \mathbb{N}_N$, *in which* $\mathcal{H}_1$ *is the space of constant function.*

Proof: Shown in Appendix A. □

In Theorem 1, we demonstrate a RKHS $\mathcal{H}_{pol}$ that contains $f_{dyn,n}$ for all $n \in \mathbb{N}_N$, because $f_{dyn,n}$ is substantially based on the Lagrangian. Moreover, $\mathcal{H}_{pol}$ is finite-dimensional, as later shown in Corollary 1, and contains the nonlinear bases in Euler-Lagrange method as a subspace.

Despite high dimensionality, the RKHS $\mathcal{H}_{pol}$ inherits computationally efficient reproducing kernel functions from (7), (8), and (9). Specifically, we propose a family of hybrid polynomial kernels parameterized by $\sigma \in [0,\infty]$ as the kernel function for $\mathcal{H}_{pol}$:

$$k_{pol}(x_i, x_j) = (k_{\ddot{q}} + (1+\sigma)^{-1} k_{\dot{q}\otimes\dot{q}}) k_{\psi\sigma}{}^2 + k_{\psi\sigma} - c_\psi , \tag{17}$$

in which

$$k_{\psi\sigma}(x_i, x_j) := c_\psi \prod_{n\in\mathbb{N}_N} (1 + \frac{\cos(q_{i,n} - q_{j,n})}{1+\sigma}) , \tag{18}$$

$c_\psi := ((2+\sigma)/(1+\sigma))^{-N}$ is chosen so that $|k_{\psi\sigma}| \le 1$. Remaining the same dimensionality, $\mathcal{H}_{pol}$'s complexity is controlled by parameter σ: with $\mathcal{H}_{pol}$ scaled by σ, the contributions of centrifugal terms and high-order trigonometric terms are penalized by the $(1+\sigma)^{-1}$ factor in (17) and (18), respectively. Because the centrifugal terms, which result from the coupling between different links, are small when a robot is equipped with a large gear ratio, k_{pol} with $\sigma \to \infty$ is designed to behave like the model linear in $\ddot{q}$, the simple mass model. Moreover, because the high-order terms in (4) correspond to the terms, usually few, not canceled by zero DH parameters (e.g. zero link offset), the parameterization in (17) serves as a good prior knowledge. In short, $\mathcal{H}_{pol}$ models general rigid-body dynamics, but, because of the computationally efficient kernel (17), it requires no derivation of complicated nonlinear bases in (4), resulting to an effective and autonomous model.

C. Convergence and Complexity of Learning

To infer the model of inverse dynamics with Hilbert space $\mathcal{H}$, we consider the error function

$$\mathcal{E}(f) := \int_{\mathcal{X}} (f(x) - y)^2 d\rho_x \tag{19}$$

and our goal is to estimate the optimal solution in $\mathcal{L}^2(\mathcal{X}, \rho_x)$

$$f_\rho := \arg\min_f \mathcal{E}(f) . \tag{20}$$

We adopt regularized least-square regression

$$\min_{f\in\mathcal{H}} \int_{\mathcal{X}} (f(x) - y)^2 d\rho_x + \gamma \|f\|_{\mathcal{H}}^2 , \tag{21}$$

in which y is the outcome and $\gamma \ge 0$ is the regularization parameter. To highlight how the hypothesis space affects learning, instead of (21), we focus on the learning algorithm

$$\min_{\|f\|_{\mathcal{H}}^2 \le R} \int_{\mathcal{X}} (f(x) - y)^2 d\rho_x , \tag{22}$$

because there exists $\gamma(R)$ such that the solutions in (21) and (22) are identical [33]. Given a RKHS $\mathcal{H}$, therefore, a natural candidate for the hypothesis space is

$$H := I_K(B_R(\mathcal{H})) , \tag{23}$$

in which $I_K : \mathcal{H} \to C(X)$ is the inclusion map in the space of continuous functions.

Suppose m observations $Z = \{(x_i, y_i)\}_{i\in\mathbb{N}_m}$ are given. Let

$$f_{\mathbf{z}} = \arg\min_{f\in\mathcal{H}} \frac{1}{m} \sum_{i\in\mathbb{N}_m} (f(x_i) - y_i)^2 + \gamma \|f\|_{\mathcal{H}}^2 . \tag{24}$$

be the empirical estimate of f_ρ in H and let $f_H := \arg\min_{f\in H} \mathcal{E}(f)$ be the optimal solution in H. By the equivalence between (21) and (22), we decompose $\mathcal{E}(f_{\mathbf{z}}) = \mathcal{E}_H(f_{\mathbf{z}}) + \mathcal{E}(f_H)$ to evaluate the model:

$$\mathcal{E}_H(f_{\mathbf{z}}) := \int_{\mathcal{X}} (f_{\mathbf{z}} - f_H)^2 d\rho_x \tag{25}$$

is the *sample error* and $\mathcal{E}(f_H)$ is the *approximation error*, which is independent of Z. Upon a further inspection, we see

$$\mathcal{E}(f_H) = \int_{\mathcal{X}} (f_H - f_\rho)^2 d\rho_x + \mathcal{E}(f_\rho) \tag{26}$$

in which $\mathcal{E}(f_\rho)$ is a constant independent of both Z and H. Because f_ρ may not be in H, $\mathcal{E}(f_H) \ge \mathcal{E}(f_\rho)$ in general. Therefore, to minimize $\mathcal{E}(f_{\mathbf{z}})$, a sufficient approach is to limit $\mathcal{E}_H(f_{\mathbf{z}})$ and $\mathcal{E}(f_H)$,

We analyze this bound by the following two theorems using covering number of the hypothesis space H.

Definition 1

Let S be a metric space and $\varepsilon > 0$. Covering number $\mathcal{N}(S, \varepsilon)$ *is the minimal number of disks in S with radius ε covering S.*

Theorem 2 [34]

Let H be a compact and convex subset in $C(\mathcal{X})$. Assume that for all $f \in H$, $|f(x) - y| \le M$ almost everywhere. Then, for all $\varepsilon > 0$,

$$\mathrm{Prob}\{\mathcal{E}_H(f_{\mathbf{z}}) \le \varepsilon\} \ge 1 - \mathcal{N}(H, \frac{\varepsilon}{24M}) \mathrm{e}^{\frac{-\varepsilon m}{288M^2}} \tag{27}$$

Theorem 3 [33]

Let k be a Mercer kernel of RKHS $\mathcal{H}$ on $\mathcal{X}$ and $L_k : \mathcal{L}^2(\mathcal{X}, \rho_x) \to \mathcal{L}^2(\mathcal{X}, \rho_x)$ be the operator given by

$$L_k f(x) = \int_{\mathcal{X}} k(x,t) f(t) d\rho_x(t), \quad x \in \mathcal{X} .$$

Let $\theta > 0$. If $f_\rho = L_k^{\theta/(4+2\theta)} g$ for some $g \in \mathcal{L}^2(\mathcal{X}, \rho_x)$, then

$$\inf_{\|f\|_{\mathcal{H}}^2 \le R} \int_{\mathcal{X}} (f - f_\rho)^2 d\rho_x \le 2^{2+\theta} \|g\|_{\mathcal{L}^2(\mathcal{X},\rho_x)}^{2+\theta} R^{-\theta} . \tag{28}$$

By taking $H = I_K(B_R(\mathcal{H}))$, Theorem 2 and Theorem 3 can be used to bound the sampling error and the approximation error, respectively. More specifically, we focus on the order of covering number and the norm

$$\|L_k^{-\theta/(4+2\theta)} f_\rho\|_{\mathcal{L}^2(\mathcal{X},\rho_x)} , \tag{29}$$

and use them to analyze RKHSs in learning the inverse dynamics model (4). Our results show a quantitative bound of covering number and a qualitative analysis of (29).

We first discuss some popular options for (4). Given that $f_{dyn,n} \in C^\infty(\mathcal{X})$ in (4), a popular RKHS candidate is $\mathcal{H}_{rbf}$ endowed with the universal kernel,

$$k_{rbf}(x_i, x_j) := \exp(-\|x_i - x_j\|^2 / 2\sigma) . \tag{30}$$

However, this appealing choice may not be ideal for learning inverse dynamics of general robots, especially those with rotary joints. This deficiency is attributable to the fact that

$$k_{rbf}(x_i, x_j) = e^{\frac{\|x_i\|^2}{2\sigma}} e^{\frac{\|x_j\|^2}{2\sigma}} \sum_{n=0}^{\infty} \frac{\langle x_i, x_j \rangle^n}{(\sigma)^n n!} \tag{31}$$

penalizes all high-order polynomial terms. If σ in (30) is large, i.e. when (29) increases, the cross-terms in (4) due to the serial structure and the terms due to trigonometric functions are particularly highly penalized. Yet a small σ easily leads to over-fitting, as shown in the following proposition.

Proposition 3 [33]

Let $x \in \mathbb{R}^d$ and $\eta > 0$, for $\mathcal{H}_{rbf}$ with the kernel defined in (30),

$$\ln \mathcal{N}(I_K(B_R(\mathcal{H})),\eta) \le n\left(32 + \frac{640d(\mathrm{Diam}(\mathcal{X}))^2}{\sigma^2}\right)^{d+1}\left(\ln\frac{R}{\mu}\right)^{d+1} \quad (32)$$

For rotary joints, the kernel (30) can be modified as

$$k_{rbfs}(x_i,x_j) := \exp\left(-\frac{\left\|\psi(q_i)-\psi(q_j)\right\|^2 + \left\|\dot{q}_i-\dot{q}_j\right\|^2 + \left\|\ddot{q}_i-\ddot{q}_j\right\|}{2\sigma}\right) \quad (33)$$

As in the proof of Theorem 1, (4) is a quadratic function of $\psi(x)$. Therefore, a large σ may exist so that (29) is small for the kernel (33). On the other hand, (33) is equivalent to a rbf kernel defined on $\mathbb{R}^{4N}$, inducing a larger variance in learning. Even so, in learning rotary robots (33) outperforms (30) mostly because the structure of (4) is considered, as evidenced in the simulations.

The RKHS $\mathcal{H}_{pol}$ with the hybrid polynomial kernel (17) features better: First, (17) considers the trigonometric bases as with (33). Second, introducing the tensor of different elementary RKHSs reduces the dimensionality, as shown in Theorem 1, selecting only partial terms of the polynomial function of degree $2N$ in $\mathbb{R}^{4N}$. Finally, the control parameter σ tailored (17) specially for robot dynamics so that the penalized subspaces have physical meanings.

We show the covering number of $I_K(B_R(\mathcal{H}_{pol}))$ by Theorem 4 with a lemma in approximation theory.

Lemma 1 [33]

Let E be an n-dimensional Banach space. For all $R > 0$, $0 < \eta < R$,

$$\ln \mathcal{N}(B_R(E),\eta) \le n \ln\left(3R/\eta\right), \quad (34)$$

and for $\eta \ge R$, $\mathcal{N}(B_R(E),\eta) = 1$.

Theorem 4

For $\mathcal{H}_{pol}$ with kernel defined in (17), the covering number of $I_K(B_R(\mathcal{H}_{pol}))$ is bounded by a non-increasing function of σ. In the limit, it resembles

$$\ln \mathcal{N}(I_K(B_R(\mathcal{H}_{pol})),\eta) \sim O(N\ln(\frac{R}{\eta})) \quad (35)$$

as $\sigma \to \infty$, and

$$\ln \mathcal{N}(I_K(B_R(\mathcal{H}_{pol})),\eta) \sim O(N^2 5^N \ln(\frac{R}{\eta})) \quad (36)$$

as $\sigma \to 0$.

Proof: Shown in Appendix B. □

Parameter σ controls the size of hypothesis space $I_K(B_R(\mathcal{H}_{pol}))$ and affects the convergence of learning. For robots with a large gear ratio or simple DH parameters, a large σ increases the convergence rate, because the effective size of the hypothesis space is smaller and (29) minimally grows given the specific penalization in (17). Conversely, for general robots, hybrid polynomial kernel (17) still benefits learning, because it captures the tendency polynomial in $\ddot{q}$ and $\dot{q}$. Therefore, this kernel is sufficient to train a descent model for high-speed applications with training data of slow trajectories. As for kernels such as (30) and (33), sufficient training data suggest trajectories with all speeds and accelerations, a setting generally impossible. Finally, Corollary 1, which follows straight from the proof of Theorem 4, shows a bound of the dimension of $\mathcal{H}_{pol}$ using trigonometric identities.

Corollary 1

For $\mathcal{H}_{pol}$ with hybrid polynomial kernel (17),

$$\dim(\mathcal{H}_{pol}) \sim O(N^2 5^N). \quad (37)$$

In particular,

$$\dim \mathcal{H}_{pol} \le (N + 2^{-1}N(N+1))5^N + 3^N - 1. \quad (38)$$

III. Learning Inverse Dynamics in a Semi-Parametric Framework

In control of holonomic robots, the inverse dynamics model is referred to as the mapping from the states of dynamics $(q,\dot{q},\ddot{q})$ to actuation force τ_a. That is, the inverse map $\Gamma : (q,\dot{q},\ddot{q}) \to \tau_a$ such that

$$\left(\frac{d}{dt}\frac{\partial}{\partial \dot{q}_n} - \frac{\partial}{\partial q_n}\right)L = \tau_n = \tau_{a,n} + \tau_{f,n} \quad (39)$$

holds for all $n \in \mathbb{N}_N$, in which τ_f denotes the force due to friction and unmodeled dynamics, and the subscript denotes the *n*th component. In presence of τ_f, especially large static friction, the inverse map Γ is poorly defined in general, whereas the inverse map from $(q,\dot{q},\ddot{q})$ to τ_n (i.e. $f_{dyn,n}$) always exists. Therefore, because the hypothesis space lies in $C(\mathcal{X})$, we can at best learn in a probably approximately correct fashion.

We adopt a semi-parametric framework to model inverse dynamics, leading to the problem

$$\min_{f\in\mathcal{H}_{dyn},b_j} \frac{1}{m}\sum_{i\in\mathbb{N}_m}(f(x_i) + \sum_{j\in\mathbb{N}_B} b_j\phi_j(x_i) - y_i)^2 + \gamma\left\|f\right\|^2_{\mathcal{H}_{dyn}}, \quad (40)$$

in which $\mathcal{H}_{dyn}$ is the RKHS for modeling rigid-body dynamics in (4), B is the number of the (nonlinear) bases $\{\phi_b\}_{b\in\mathbb{N}_B}$ that are not regularized, and b_j represents the coefficients to be identified. Because $B << \dim(H)$, over-fitting due to parametric bases does not occur. For friction, we use the bases

$$\{\dot{q}_n, \tanh(\dot{q}_{i,n}/\sigma_f), 1\} \quad (41)$$

to model viscous friction and coulomb friction of joint *n*, in which σ_f is the additional parameter for controlling the Lipschitz constant of the sigmoid function. Given that (41) are continuous functions, a RKHS $\mathcal{H}_{fri}$ with kernel function k_{fri} that contains (41) exists; for example,

$$k_{fri}(x_i,x_j) = \dot{q}_{i,n}\dot{q}_{j,n} + \tanh(\dot{q}_{i,n}/\sigma_f)\tanh(\dot{q}_{j,n}/\sigma_f) + 1. \quad (42)$$

In addition to (41), the basis of rigid-body dynamics with known kinematics [6] can also be included to improve the performance as in [17], using $\mathcal{H}_{dyn}$ to correct kinematic errors. In the succeeding simulations and experiments, we consider only parametric bases in (41), because we want to show that the proposed structured kernels (17) alone yield comparable performance.

To numerically solve (40), we cast the semi-parametric framework (40) into a multiple kernel formulation:

$$\begin{aligned}&\min_{f\in\mathcal{H}_{dyn}\oplus\mathcal{H}_{fri}}\frac{1}{m}\sum_{i\in\mathbb{N}_m}(f(x_i)-y_i)^2+\gamma((1-\delta)\|f\|^2_{\mathcal{H}_{dyn}}+\delta\|f\|^2_{\mathcal{H}_{fri}})\\ &=\min_{f\in\mathcal{H}_{dyn}\oplus\mathcal{H}_{fri}}\frac{1}{m}\sum_{i\in\mathbb{N}_m}(f(x_i)-y_i)^2+\gamma\|f\|^2_{\mathcal{H}_{dyn}\oplus\mathcal{H}_{fri}}\end{aligned} \tag{43}$$

for some $0<\delta<<1$, in which the effective kernel function of $\mathcal{H}_{dyn}\oplus\mathcal{H}_{fri}$ is then

$$k_{dyn\oplus fri}=(1-\delta)^{-1}k_{dyn}+\delta^{-1}k_{fri}\,. \tag{44}$$

Therefore, the regularized least-square in (24) can be used with kernel function (44) to solve (40), which is numerically equivalent to the linear system

$$(m\gamma\mathbf{I}+\mathbf{K}_{dyn\oplus fri})\boldsymbol{\alpha}=\mathbf{y} \tag{45}$$

giving the estimated model in the form of

$$f_{\mathbf{z}}(x)=\sum_{i\in\mathbb{N}_m}\alpha_i k_{dyn\oplus fri}(x,x_i)\,, \tag{46}$$

in which $\boldsymbol{\alpha}=(\alpha_i)_{i\in\mathbb{N}_m}$ are the coefficients to be identified, $\mathbf{y}=(y_i)_{i\in\mathbb{N}_m}$, and $\mathbf{K}_{dyn\oplus fri}=(k_{dyn\oplus fri}(x_i,x_j))_{i,j\in\mathbb{N}_m}$.

In evaluation, we rearrange the solution (46) back into the semi-parametric form. That is, to recover the unknown coefficient b_j in (40) from (46) by

$$b_j=\delta^{-1}\sum_{i\in\mathbb{N}_m}\alpha_i\phi_j(x_i)\,. \tag{47}$$

Therefore, only k_{dyn} is necessary for evaluating (46), i.e.

$$f_{\mathbf{z}}(x)=(1-\delta)^{-1}\sum_{i\in\mathbb{N}_m}\alpha_i k_{dyn}(x,x_i)+\sum_{j\in\mathbb{N}_B}b_j\phi_j(x)\,, \tag{48}$$

which considerably increases efficiency, especially for online applications.

The representation in (46) holds, which approximates the solution of (40), as long as $\delta>0$. For $\delta=0$, there exists $\beta_i\neq\alpha_i$ satisfying

$$f_{\mathbf{z}}(x)=(1-\delta)^{-1}\sum_{i\in\mathbb{N}_m}\alpha_i k_{dyn}(x,x_i)+\beta_i k_{fri}(x,x_i)\,, \tag{49}$$

in which β_i is finite with equivalence

$$b_j=\sum_{i\in\mathbb{N}_m}\beta_i\phi_j(x_i)\,. \tag{50}$$

Finally, we prove that the semi-parametric framework is consistent in learning.

Theorem 5

For holonomic rigid-body robots, let y be the random variable $\tau_n-\tau_{f,n}$, $f_{\mathbf{z}}$ *be the solution of (40), and*

$$f_{H,pol}:=\arg\min_{f\in\mathcal{H}_{pol}}\min_{b_j}\int_{\mathcal{X}}(f+\sum_{j\in\mathbb{N}_B}b_j\phi_j-y)^2d\rho_x\,. \tag{51}$$

Assume $|y|<\infty$ *almost everywhere. Then there exist* $\xi,\gamma_0>0$ *such that with probability* $1-\xi$, $\|f_{H,pol}-f_{\mathbf{z}}\|_{\mathcal{H}_{pol}}\leq\varepsilon(m,\sigma)$ *for all* $\gamma<\gamma_0$, *in which* $\varepsilon(m,\sigma)$ *is a monotonically decreasing function of m and a non-increasing function of* σ. *Thus,* $\lim_{m\to\infty}\varepsilon(m,\sigma)=0$.

Proof: To prove the convergence of (40), we analyse the convergence of (43) in the direct-summed RKHS $\mathcal{H}_{pol}\oplus\mathcal{H}_{fri}$ by showing that the solution of (51) has a finite representation $f_{H,pol}$ in $\mathcal{H}_{pol}\oplus\mathcal{H}_{fri}$, and that the solution of (43) converges to $f_{H,pol}$ by Theorem 2. Then, by the equivalence between (40) and (43), the solution of (40) is consistent.

Let $f_{H,pol}=f_{pol}+f_{fri}$. Because $\dim(\mathcal{H}_{pol})<\infty$ and $B<\infty$, there exists finite $f_{pol}\in\mathcal{H}_{pol}$ and $f_{fri}\in\mathcal{H}_{fri}$ such that $f_{H,pol}$ represents the solution of (51); by definition of $\|\cdot\|_{\mathcal{H}_{pol}\oplus\mathcal{H}_{fri}}$ in (43), that is, $\|f_H\|_{\mathcal{H}_{pol}\oplus\mathcal{H}_{fri}}<\infty$.

As a result, because of the connection between (21) and (22), there exists $\gamma_0>0$, such that for all $\gamma<\gamma_0$ the solution of (21) is in accordance with finite solution in hypothesis space $H=I_K(B_R(\mathcal{H}_{pol}\oplus\mathcal{H}_{fri}))$ with $\|f_{H,pol}\|_{\mathcal{H}_{pol}\oplus\mathcal{H}_{fri}}<R<\infty$.

Finally, by Theorem 2, taking

$$\xi=\mathcal{N}(H,\frac{\varepsilon}{24M})e^{\frac{-\varepsilon m}{288M^2}}=e^{C_\sigma N^2\ln(\frac{24MR}{\varepsilon})}e^{\frac{-\varepsilon m}{288M^2}} \tag{52}$$

in which $C_\sigma>0$ is a non-increasing function of σ, independent of M, R, and ε, and using the lower bound of (52),

$$\begin{aligned}-\ln\xi&=C_\sigma N^2\ln(\frac{\varepsilon}{24MR})+\frac{\varepsilon m}{288M^2}\\ &\geq C_\sigma N^2\ln(\frac{\varepsilon}{24MR})+\ln\frac{\varepsilon m}{288M^2}\end{aligned} \tag{53}$$

we have

$$\varepsilon\leq(24MR)^{\frac{C_\sigma N^2}{1+C_\sigma N^2}}(\frac{\xi m}{288M^2})^{\frac{-1}{1+C_\sigma N^2}}\,. \qquad \square$$

IV. SIMULATIONS

We compare the generalization of the structured kernel (17), the modified rbf kernel (33), and the traditional rbf kernel (30) in learning inverse dynamics of rigid-body robot. In each of the following simulations, we show testing error with respect to the complexity of the underlying model, i.e. the robot's DOF, in different scenarios: with or without the presence of measurement noise and friction. For each DOF, 10 different robots are used as the target to be learned, whose kinematic and dynamic parameters, gear ratios, and friction magnitude are uniformly sampled from a bounded set so that all these robots are physically feasible (e.g. the inertia matrix is always positive definite). For each robot, $m=500$ training data and $m_{val}=15000$ validating data, with angular positions, angular velocities, and angular accelerations sampled from a bounded uniform distribution, are generated by Newton-Euler method; for comparison, the torque τ is normalized so that $\|\tau\|_\infty\leq 1$. The adopted noise, which shares the same unit as the normalized torque, is a zero-mean Gaussian with standard variation 0.05; with different joints independently modeled, the Coulomb friction is modeled as sign function, and the viscous friction is modeled by a force linear in joint velocity.

To learn the unknown model, we use regularized least-square regression in (24) and the parameters σ , σ_f , and γ are chosen by 5-fold cross validation, if not particularly specified; δ is fixed as $10^{-3} trace(\mathbf{K}_{dyn}) / trace(\mathbf{K}_{fri})$, in which $\mathbf{K}_{dyn} \in \mathbb{R}^{m\times m}$ and $\mathbf{K}_{fri} \in \mathbb{R}^{m\times m}$ are the empirical kernel matrices. The optimal parameters, with which the entire training data set used to re-train the final model, are chosen to be the combination of parameters that minimizes the empirically expected prediction error. To verify the result, the performance is illustrated in terms of prediction errors over all the generalized coordinates in root-mean-square (RMS), i.e. $N^{-1/2}\left\| y_i - f_{\mathbf{z}}(x_i)\right\|$.

In learning without kinematic information, *pol* denotes the proposed kernel (17), *rbf* denotes (30), *rbfs* denotes (33), and *fri* denotes (42); the notation + is used to combine two kernels in the form of (44), in which the first argument is $\mathcal{H}_{dyn}$ and the second argument is $\mathcal{H}_{fri}$. Also, for benchmark, we take *motor*, a simple independent joint model,

$$c_1\ddot{q}_n + c_2\dot{q}_n \, , \tag{54}$$

in which c_1 and c_2 are the unknowns to be identified for joint *n*. We do not use Euler-Lagrange model, because it can be exponentially complex for general robots.

Fig.1 shows predicting the ideal robot dynamics without any friction and noise, in which we fixed $\gamma = 10^{-12}$ in (24) and searched parameter σ by cross validation. Recalling the bound of the dimensionality of $\mathcal{H}_{pol}$ in (38), we can see that Fig. 1.(b) shows uniform convergence for $N \le 2$ in $\mathcal{H}_{pol}$, because 500 training data are sufficient to span the entire space. Conversely, for $N > 2$, the generalization is dominated by regularization. In this situation, the performance of a kernel depends on the quality of the regularized parameters, i.e. σ in each kernel function. In comparison, *rbfs* outperforms the traditional *rbf*, because it better captures the characteristics of the rotary joints, so that a hypothesis space with both small covering number and (29) is possible. And the proposed kernel *pol* shows the best performance because of its special structure.

Fig.2 shows predicting the ideal robot dynamics with both friction and noise, in which the Coulomb friction and the viscous friction are modeled with the magnitude randomly chosen as mentioned. Compared with the finding in Fig.1, that in Fig. 2 indicates that the kernel *pol* alone exhibits poor performance in the presence of friction at small N . Its performance increases, however, by introducing *fri*. Given that *pol*+*fri* captures the structure of the dynamics, its performance is consistently better than that of *rbf* and *rbfs*. Another feature is that all the models learn similarly as N increases, because the coupling of different links dominates the effect of friction. Overall, *pol*+*fri* learns, as if no friction exists, consistently exhibiting better performance than *rbf* and *rbfs*.

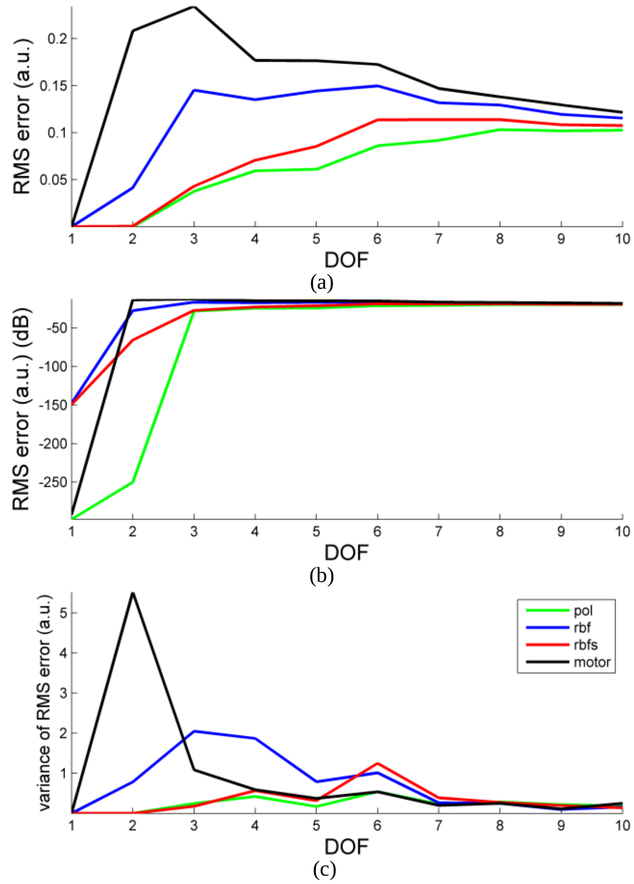

Fig. 1. RMS error of prediction in learning the ideal model. (a) RMS error (b) RMS error in dB $20\log(\cdot)$ (c) the variance of RMS .error, where a.u. denotes arbitrary unit.

V. Experiments

The models were empirically validated in experiments with the 6-DOF NTU robot arm (NTU Robotics Laboratory) in Fig. 3, which is a 6-DOF robotic manipulator driven by DC-micromotors with large gear ratios. With current sensors and encoders, the robot arm is fed back by a 10-kHz inner torque PI-controller and a 250-Hz outer position PD-controller, and can be feedforwarded with additional torque command. To collect training data, we used 10 trajectories (interpolated by a 5th-order polynomial; sampled at 500 Hz) that randomly, smoothly traverse all workspace at different speeds for approximately 30-40 seconds, and recorded the trajectory tracking experiments of 6-DOF NTU robot arm with PD position feedback. To compute $\dot{q}$ and $\ddot{q}$, the sampled trajectories were filtered with a 3rd-order Butterworth filter and then differentiated.

Blocked cross validation [35] was adopted in the experiments, which is commonly used in time-series prediction. By blocking the training data in time domain into equal-sized groups, a particular set of parameters was scored by carrying out conventional cross validation in terms of the groups. Because the i.i.d. assumption is likely to be satisfied in terms of such partition, blocked cross validation enables correct and unbiased parameter selection, provided that the block is large enough.

To validate the models, we compare prediction torque error

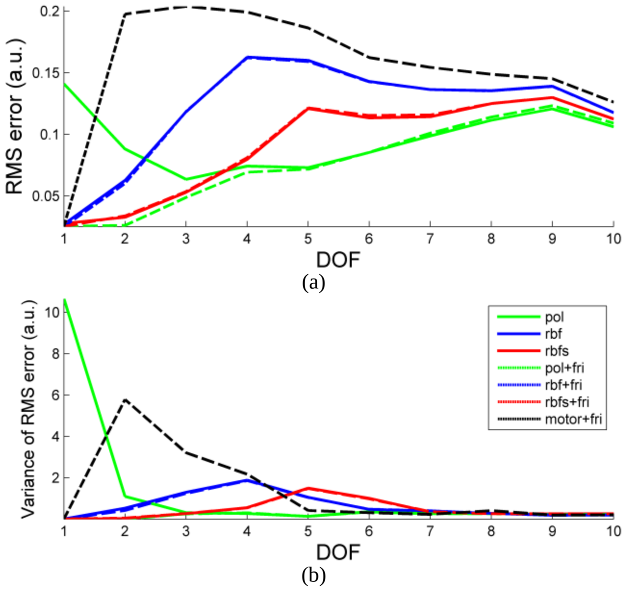

Fig. 2. RMS error of prediction in learning the ideal model with simulated friction and Gaussian measurement noise. (a) mean (b) variance.

Fig. 3. 6-DOF NTU robot arm.

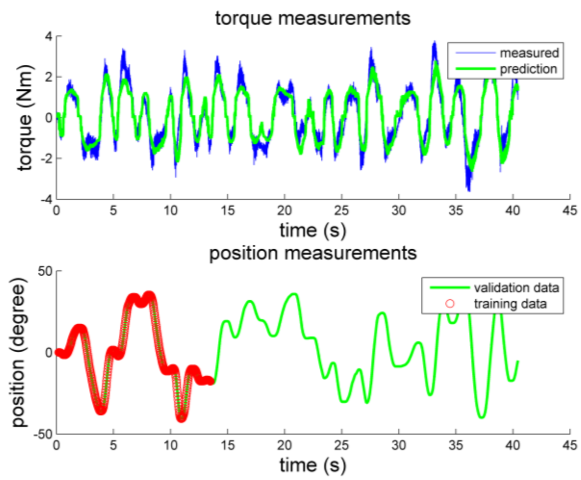

Fig. 4. The collected data and the prediction of *pol+fri* of joint 3. Each model is trained with the first 1/3 of the collected data, and tested on the rest 2/3. The validation trajectories traverse the workspace with a speed gradually ascending.

and position tracking error in pre-computed torque control [36] with the learned model. To unbiasedly estimate prediction error, we, using a 5-fold 3-second blocked cross validation, trained the model with only 500 samples from the first 1/3 of each trajectory in time domain, and tested the prediction torque with the validation set composing of the remaining 2/3 of the data, as illustrated in Fig.4. Therefore, this score more faithfully reflects how a model performs in applications where training data over the entire workspace is prohibited. While Fig. 4 exemplifies the performance of a single prediction, Fig. 5 summarizes the torque predictions of all trajectories in RMS error. Because the friction in the 6-DOF NTU robot arm is large, indicating that a single kernel standalone does not provide satisfactory results, the semi-parametric framework considerably increases accuracy by introducing the simple basis *fri* for friction.

In addition to prediction, we conducted experiments with pre-computed torque control using the learned models. In these experiments, 500 samples from the first 1/3 of each trajectory were used to train the models, and then tracking experiments of the whole trajectory with the 6-DOF NTU robot arm were conducted using PD feedback and the feedforward terms predicted by the learned models. Given that the first 1/3 of the data were used in learning, only the position tracking errors of the remaining 2/3 of a trajectory were used in evaluation. We note that the magnitude of the PD gain was purposely tuned small to contrast the tracking results with and without the feedforward term, and therefore the absolute tracking error bears little significance. In consequence, these figures (Fig. 5–8) serve rather as a profile for qualitative analysis.

Fig. 6 shows the RMS errors of tracking the trajectories used in Fig. 5 with precomputed feedforward compensation. The results majorly fall into three groups: feedback only (denoted as *none*), feedforward without friction model, and feedforward with friction model. These results evidence the importance of the semi-parametric model; however, because multiple factors were involved, as explained in section VI, the discrimination between the models is less obvious than that in Fig. 5.

Fig. 7 and Fig. 8 further present the tracking results of the model *pol+fri*, which also learned from the first 1/3 of the training data and then predicted the feedforward term for the whole trajectory. Fig. 7 shows the result of tracking a square trajectory in the Cartesian space. In this experiment, the PD gain was tuned 1/3 of that used in the experiments in Fig. 6 and Fig. 8, so that the tracking without feedforward term (denoted as *none*) becomes undesirable and more discernable. Under this extreme condition, despite imperfection, using the model that learned from limited observations still largely decreases the tracking error. To further investigate the property of each joint, Fig. 8 shows the result of tracking another joint-space trajectory that was generated randomly in same way as the data used in Fig. 5 and Fig. 6. In this experiment, the PD gain was the same as that in Fig. 6. As shown in these figures, the importance of the feedforward term depends on the dynamics of the joint: for joints with large coupled terms or friction (e.g. joint 2–5), the improvement is more significant.

VI. Discussions

In the experiments, we adopted blocked cross validation instead of standard cross validation. Given that cross validation relies on i.i.d. assumption that the testing data (including posi-

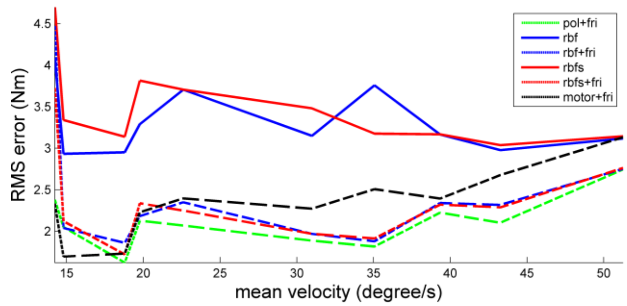

Fig. 5. RMS error of torque prediction in experiments, evaluated on the remaining 2/3 of collected data.

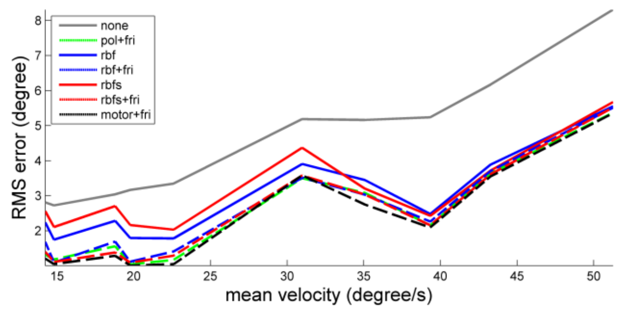

Fig. 6. RMS error of position trajectories in experiments, evaluated on the remaining 2/3 of collected data (*none* denotes PD position feedback alone).

tion, velocity, and acceleration) share the same probability distribution as the training data, learning-based methods often fail to choose the correct parameters if standard cross validation is employed. More specifically, the parameter selected by standard cross-validation tends to overfit the data, because the collected data are dependent over time, traveling on a manifold in forward dynamics. Underestimating the support of ρ_x, it optimistically assumes that the potential data in the succeeding application have the same probability distribution as the collected data. However, such assumption typically does not hold in identifying dynamics, because available observations are finite and the size of $\mathcal{X}$ is exponential in N.

For a similar reason, we used the first 1/3 of the data for training and evaluated the error on the last 2/3. Separating the training and the validation data in time domain gives a more unbiased estimate of the model's performance (of both prediction and tracking). On the other hand, because of the strong time-domain correlation, uniform sampling results in an over-estimated performance, only suitable for iterative learning control where over-fitting becomes rather a merit.

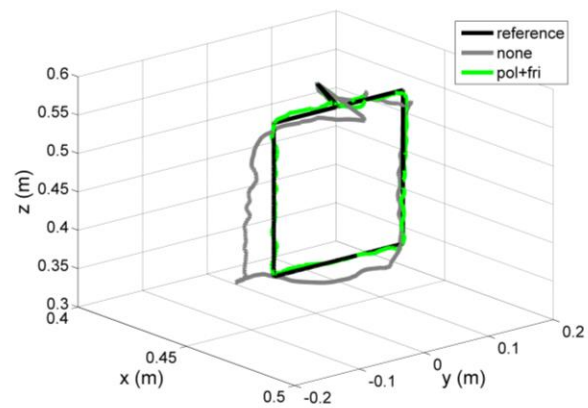

Fig. 7. The results of tracking a square trajectory (*none* denotes PD position feedback alone).

The factors involved in pre-computed torque control are more complicated. Given that an appropriate feedforward term theoretically linearizes the system, two primary factors affect the outcome. First, the maximum output torque of the actuator is limited. Therefore, the controller cannot eliminate the effects of robot dynamics even if the feedforward term is ideally correct, making the position deviate from the predefined trajectory. Second, pre-computed compensation (as opposed to computed-torque control which cancels the whole dynamics with online feedback) may be different from the torque needed when the accumulated errors drive the current state far from the supposed state in the reference trajectory. This leads to a conundrum in presenting the tracking results: using a simple feedback with limited gain can better distinguish the performance of different models yet introduces other tracking errors, which may be larger the difference. As a result, we present Fig. 6 rather qualitatively and consider only a single trajectory in Fig. 7 for demonstration purpose.

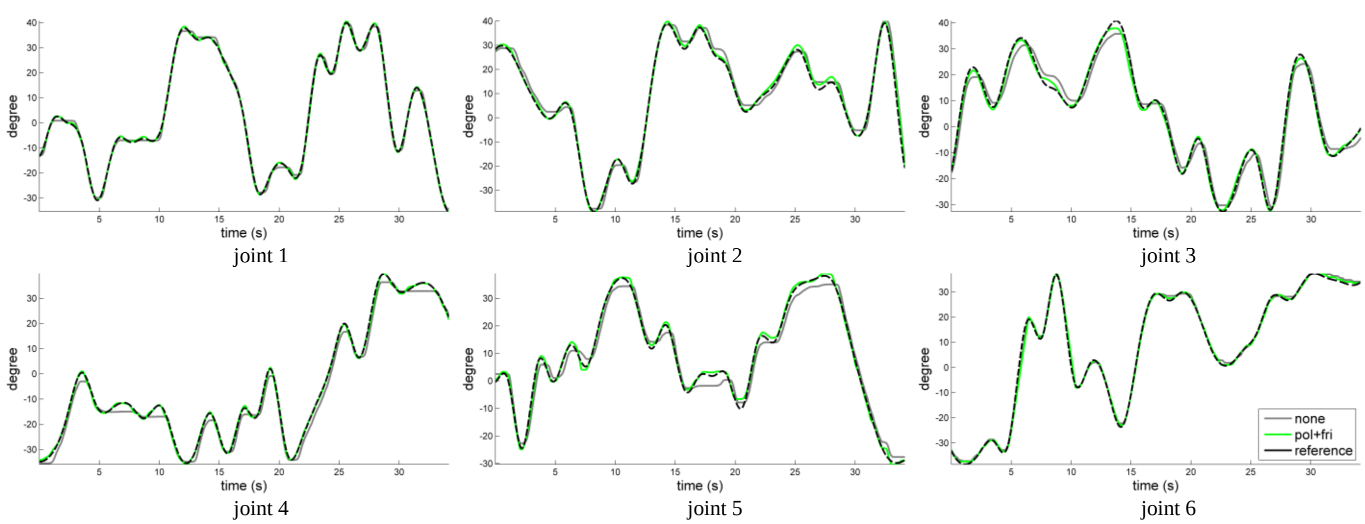

Fig. 8. The results of tracking a joint-space trajectory that transverses through randomly selected points over the workspace (*none* denotes PD position feedback alone).

In summary, the simulations and the experiments mainly demonstrate two trends: kernels sharing a structure similar to robot dynamics generalize better to unseen data; compensating friction, the semi-parametric framework significantly improves the performance, especially if friction is too large to disregard.

In terms of generalization, the proposed *pol* kernel, which converges to the same function as Euler-Lagrange method without explicit evaluation of the nonlinear bases, surpasses general kernels. According to the analysis in Section II.C, the generalization is mainly affected by the covering number of the hypothesis space. Therefore, with its dimensionality decreased by its structure resembling Euler-Lagrange model and the corresponding covering number regularized by physically meaningful σ , the kernel *pol* effectively generalizes to rest of the data, though the model learns only form partial data (similarly, for robots with rotary joints, kernel *rbfs* is a better choice than *rbf*).

However, *pol*, or even *rbf* and *rbfs*, alone may yield unsatisfactory results when friction is relatively large. In this case, we suggest the semi-parametric framework as it effectively boosted the performance of all kernels, in particular *pol+fri*. This effect can be observed in both of the simulations and the experiments: in the simulations, the performance of *pol* improves significantly in Fig. 2, nearly to that without friction; in the experiments, the performance of all kernels improves, especially at low speed where friction is large compared with the size of dynamics.

To better illustrate, we can further compare the results with the simple model *motor+fri*. As previously stated, the NTU robot arm has large gear ratios, and therefore the system behaves similarly to the independent-joint model, as long as the robot operates slow enough to generate non-significant coupled dynamics. Thus, we can treat the simple motor model in (54) as benchmark. In Fig. 5, *motor+fri* overtakes the other models at very low speed, whereas *pol+fri* yields more satisfactory results generally, especially in high-speed trajectories; *rbfs* performs worse than *rbf*, in contrast to the simulated results in Fig. 1 and 2. All these differences are explained by the size of friction: when robot dynamics dominate, the kernels perform similarly as with Fig. 1 or as with robots with large DOF in Fig. 2; when friction dominates, the kernels maintain the original performance, only if friction can be compensated by additional parametric basis. Therefore, the success of the semi-parametric framework can be attributed to that the RKHSs in which the hypothesis space has small covering number are different for robot dynamics and friction.

For future applications, we would incorporate the nominal plant (derived from CAD or rigid-body model with un-calibrated kinematic information) as part of the parametric basis in the semi-parametric framework, and use the proposed kernel k_{pol} to learn the error dynamics. Given that a good nominal plant reduces the norm of the unknown in the RKHS, the covering number of the hypothesis space decreases, thereby generalizing better.

Another practical adaption is to use a modified *pol* kernel,

$$\tilde{k}_{pol} = (k_{\ddot{q}} + (1+\sigma)^{-1} k_{\dot{q}\otimes\dot{q}}) k_{\psi\sigma}{}^{2}, \qquad (55)$$

which does not consider gravity, with the parametric basis for gravity derived from Euler-Lagrange method using (2). We tailor this fusion especially for robots whose dynamics are dominated by quasi-static approximation and floating-base robots (e.g. humanoids), in which the gravity vector varies with regard to the robot's base. Instead of using the original (17) which assumes stationary gravitational filed, this fusion distinguishes the gravity part, which possesses efficient parametric bases elementary to derive, and the kinetic part, which contributes to the main burden in Euler-Lagrange method. As a result, a robot can not only learn automatically without kinematic information, but also adjust in accordance to the information of gravity force.

VII. Conclusion

Circumventing the exact evaluation of parametric function, learning in RKHS is an efficient technique to approximate continuous functions. We propose a finite-dimensional RKHS $\mathcal{H}_{pol}$ that uniformly converges to rigid-body dynamics with controllable complexity. Endowed with the structure inherited from rigid-body dynamics and the efficient kernel representation, the proposed structured kernels enjoy the advantage of both rigid-body and learning-based models, not only as a user-friendly alternative but as an upgrade for existing identification tools.

Acknowledgment

This work is partially supported by Industrial Technology Research Institute, R. O. C. under grant C353C41210.

Appendix A (Proof of Theorem 1)

To prove Theorem 1, recall that the RKHS $\mathcal{H}_{\psi}$ is isometrically isomorphic to the feature space defined in the proof of Proposition 1. Therefore, by applying T_n on the spaces $\mathcal{H}_T$ and $\mathcal{H}_U$, we can derive the explicit form of $\mathcal{H}_{pol}$.

Let the Lagrange function L be composed of L_1, L_2 , and L_3 as

$$L = L_1 \otimes L_2 \oplus L_3 \in \mathcal{H}_{\dot{q}\otimes\dot{q}} \otimes (\mathcal{H}_{\psi} \otimes \mathcal{H}_{\psi}) \oplus \mathcal{H}_{\psi}. \qquad (A1)$$

With the abuse of notations, define $\psi(q_n) := (\cos q_n, \sin q_n, 1)$ and $\psi_2 := \psi \otimes \psi$, in which $\otimes$ denotes the tensor product. Because $\mathcal{H}_T$ and $\mathcal{H}_U$ are composed of $\mathcal{H}_{\ddot{q}}$, $\mathcal{H}_{\dot{q}\otimes\dot{q}}$, and $\mathcal{H}_{\psi}$, the image of the linear operator T_n can be identified by reproducing property,

$$\tau_n = T_n[\langle L_1, \dot{q}\otimes\dot{q}\rangle \langle L_2, \psi_2\rangle + \langle L_3, \psi\rangle]. \qquad (A2)$$

For convenience, we use $\otimes$ as the Kronecker product when considering vectors in finite dimensional space; we also neglect the normalization factor N^{-1} here, because it is not the norm but rather the span of vector space is concerned.

We first see that

$$\frac{d}{dt}\frac{\partial L}{\partial \dot{q}_n} = \underbrace{\left\langle L_1, \frac{d}{dt}\frac{\partial}{\partial \dot{q}_n} \dot{q}\otimes\dot{q} \right\rangle \langle L_2, \psi_2\rangle}_{(a)} + \underbrace{\left\langle L_1, \frac{\partial}{\partial \dot{q}_n} \dot{q}\otimes\dot{q} \right\rangle \left\langle L_2, \frac{d}{dt}\psi_2 \right\rangle}_{(b)} \qquad (A3)$$

Because

$$\frac{d}{dt}\frac{\partial}{\partial \dot{q}_n}\dot{q}\otimes\dot{q}=(\ddot{q}\otimes e_n)+(e_n\otimes\ddot{q}) \quad \text{(A4)}$$

and

$$\frac{d}{dt}\psi_2=\sum_{i\in\mathbb{N}_N}\psi_2(q_1)\otimes...\otimes\dot{q}_i\ [D\otimes I_3+I_3\otimes D]\psi_2(q_i)\otimes...\otimes\psi_2(q_N) \quad \text{(A5)}$$

we have

$$(a)=\left\langle L_1,(e_n\otimes I_N+I_N\otimes e_n)\ddot{q}\right\rangle\left\langle L_2,\psi_2\right\rangle \quad \text{(A6)}$$

$$(b)=\sum_{i\in\mathbb{N}_N}\left\langle L_1,[e_i^T\otimes(e_n\otimes I_n+I_n\otimes e_n)]\dot{q}\otimes\dot{q}\right\rangle \quad \text{(A7)}$$

$$\left\langle L_2,\psi_2(q_1)\otimes...\otimes[D\otimes I_3+I_3\otimes D]\psi_2(q_i)\otimes...\otimes\psi_2(q_N)\right\rangle$$

in which $D:=[0\ \text{-}1\ \ 0;\ 1\ 0\ 0;\ 0\ 0\ 0]$. Similarly,

$$\frac{\partial L}{\partial q_n}=\underbrace{\left\langle L_1,\dot{q}\otimes\dot{q}\right\rangle\left\langle L_2,\frac{\partial}{\partial q_n}\psi_2\right\rangle}_{(c)}+\underbrace{\left\langle L_3,\frac{\partial}{\partial q_n}\psi\right\rangle}_{(d)} \quad \text{(A8).}$$

in which

$$(c)=\left\langle L_1,\dot{q}\otimes\dot{q}\right\rangle+ \quad \text{(A9)}$$

$$\left\langle L_2,\psi_2(q_1)\otimes...\otimes[D\otimes I_3+I_3\otimes D]\psi_2(q_n)\otimes...\otimes\psi_2(q_N)\right\rangle$$

$$(d)=\left\langle L_3,\psi(q_1)\otimes...\otimes D\psi(q_n)\otimes...\otimes\psi(q_N)\right\rangle. \quad \text{(A10)}$$

By using the adjoint of the operators in (a), (b), (c), and (d), it is clear that for all $n\in\mathbb{N}_N$

$$\tau_n=(\left\langle\tau_{n1},\ddot{q}\right\rangle+\left\langle\tau_{n2},\dot{q}\otimes\dot{q}\right\rangle)\left\langle\tau_{n3},\psi_2\right\rangle+\left\langle\tau_{n4},\psi\right\rangle \quad \text{(A11)}$$

for some vectors τ_{n1} , τ_{n2} , τ_{n3} , and τ_{n4} . That is, τ_n is in

$$(\mathcal{H}_{\ddot{q}}\oplus\mathcal{H}_{\dot{q}\otimes\dot{q}})\otimes(\mathcal{H}_{\psi}\otimes\mathcal{H}_{\psi})\oplus\mathcal{H}_{\psi}$$

Finally, since the differentiation operator projects out the space of constant function, $\tau_n\in\mathcal{H}_{pol}$ for all $n\in\mathbb{N}_N$. □

Appendix B (Proof of Theorem 4)

The covering number of the compact subset $H=I_K(B_R(\mathcal{H}_{pol}))$ can be estimated by virtue of the maximal covering number of the subspaces that compose RKHS $\mathcal{H}_{pol}$ by direct sum. Let $\|\dot{q}\|_\infty\le 1$ and $\|\ddot{q}\|_\infty\le 1$ for all $x\in\mathcal{X}$. Consider an arbitrary element $f=f_{\ddot{q}}\oplus f_{\dot{q}}\oplus f_q\in\mathcal{H}_{pol}$ in H , in which $f_{\ddot{q}}\in\mathcal{H}_{\ddot{q}}\otimes(\mathcal{H}_\psi\otimes\mathcal{H}_\psi)$, $f_{\dot{q}}\in\mathcal{H}_{\dot{q}\otimes\dot{q}}\otimes(\mathcal{H}_\psi\otimes\mathcal{H}_\psi)$, and $f_q\in\mathcal{H}_\psi\setminus\mathcal{H}_1$. If $\mathcal{N}(H,\eta)\le\ell$, then there exists $F=\{f_i\}_{i\in\mathbb{N}_\ell}\in H$ such that $\forall f\in H$

$$\|f-f_i\|_{C(\mathcal{X})}:=\sup_{x\in\mathcal{X}}|f(x)-f_i(x)|\le\eta\ ; \quad \text{(B1)}$$

a sufficient condition for (B1) is

$$|(k_{\ddot{q}}k_{\psi\sigma}^2)(f_{\ddot{q}}-f_{i,\ddot{q}})|\le\eta/3 \quad \text{(B2)}$$

$$|(k_{\dot{q}\otimes\dot{q}}k_{\psi\sigma}^2)(f_{\dot{q}}-f_{i,\dot{q}})|\le\eta/3 \quad \text{(B3)}$$

$$|(k_{\psi\sigma}-c_\psi)(f_q-f_{i,q})|\le\eta/3\,. \quad \text{(B4)}$$

That is, the covering number of H is bounded by ℓ that is required for (B2), (B3), and (B4).

Let $\theta:=(1+\sigma)^{-1}\in[0,1]$. First, to estimate the required ℓ for (B4), we decompose $k_{\chi\sigma}$ into

$$k_{\psi\sigma}(x_i,x_j)=c_\psi(1+\sum_{n\in\mathbb{N}_N}\theta^n\prod_{p\in\mathbb{N}_{N,n}}\cos(\Delta q_p)) \quad \text{(B5)}$$

in which $\mathbb{N}_{N,n}$ denotes the set of all subsets of $\mathbb{N}_N$ with cardinality n , and $\Delta q_p:=q_{i,p}-q_{j,p}$. We treat $k_{\psi\sigma}$ as the inner product of the direct sum of subspaces. These spaces are the 1-dimenisonal space of the constant function, and the other, for $n\in\mathbb{N}_N$, 2^n-dimensional subspaces with multiplicity $C(N,n)$ of trigonometric functions, because

$$\cos(\Delta q_p)=\cos q_{i,p}\cos q_{j,p}+\sin q_{i,p}\sin q_{j,p} \quad \text{(B6)}$$

can be treated as inner product in $\mathbb{R}^2$. Therefore, a sufficient condition for (B4)is

$$\|(f_{q,j}-f_{i,q,j})\|_{\mathcal{H}_j}\le\frac{\eta/3}{\#(k_{\psi\sigma})\|k_{\psi\sigma,j}\|_{C(\mathcal{X})}}\,, \quad \text{(B7)}$$

for all the subspaces with kernel $k_{\psi\sigma,j}$ in (B5), in which $j\in\mathbb{N}_{\#(k_{\psi\sigma})}$ and

$$\#(k_{\psi\sigma})=1+\sum_{n\in\mathbb{N}_N}C(N,n)=2^N\,, \quad \text{(B8)}$$

is number of subspaces in (B5). With Lemma 1, we know ℓ that satisfies (B4) can be bounded by

$$\ln\ell\le\max_{n\in\mathbb{N}_N}2^n\ln(\frac{9R}{\eta}2^N(1+\theta)^N\theta^n)\,. \quad \text{(B9)}$$

For (B2) and (B3), we decompose $k_{\psi\sigma}^2$ as

$$\begin{aligned}k_{\psi\sigma}^2(x_i,x_j)&=c_\psi^2\prod_{n\in\mathbb{N}_N}(\frac{1+\cos(2\Delta q_n)}{2}\theta^2+2\theta\cos(\Delta q_n)+1)\\&=c_\psi^2[1+\sum_{n\in\mathbb{N}_N}\theta^n\prod_{p\in\mathbb{N}_{N,n}}(2\cos(\Delta q_n)+\theta\frac{1+\cos(2\Delta q_n)}{2})]\end{aligned} \quad \text{(B10)}$$

which are similar to (B5). Using (B6), we know (B10) is the direct sum of the 1-dimeniosnal subspace of the constant function and the 5^n-dimensional subspaces with multiplicity $C(N,n)$ for $n\in\mathbb{N}_N$; thus $\#(k_{\psi\sigma}^2)=2^N$. With Lemma 1, we have the bound

$$\ln\ell\le N\max\{1,\max_{n\in\mathbb{N}_N}5^n\ln(\frac{9R}{\eta}2^N(1+\theta)^N(2+\theta)^n\theta^n)\} \quad \text{(B11)}$$

for (B2) and the bound

$$\ln\ell\le\frac{N(N+1)}{2}\max\{1,\max_{n\in\mathbb{N}_N}5^n\ln(\frac{9R}{\eta}2^N(1+\theta)^N(2+\theta)^n\theta^{n+1})\} \quad \text{(B12)}$$

for (B3). Thus, it is sufficient to have ℓ balls with radius η covering H ; ℓ is bounded by the maximum of (B9), (B11) and (B12). Also, it is obvious to show this bound is a non-decreasing function of θ , i.e. a non-increasing function of σ . □

References

[1] S. Chiaverini, B. Siciliano, and L. Villani, "A survey of robot interaction control schemes with experimental comparison," *IEEE/ASME Trans. Mechatron.*, vol. 4, pp. 273-285, Sep. 1999.

[2] X. An, C. G. Atkeson, J. D. Griffiths, and J. M. Hollerbach, "Experimental evaluation of feedforward and computed torque control," *IEEE Trans. Robot. Autom.*, vol. 5, Jun. 1989.

[3] C. Ott, *Cartesian Impedance Control of Redundant and Flexible-Joint Robots* vol. 49. New York: Springer, 2008.

[4] T.-H. Huang, C.-A. Cheng, and H.-P. Huang, "Self-learning assistive exoskeleton with sliding mode admittance control," in *IEEE/RSJ Int. Conf. Intelligent Robots and Systems*, Tokyo, Japan, 2013, pp. 698-703.

[5] F. Reyes and R. Kelly, "On parameter identification of robot manipulators " in *Int. Conf. Robotics and Automation*, Albuquerque, New Mexico, 1997, pp. 1910-1915.

[6] C. G. Atkeson, C. H. An, and J. M. Hollerbach, "Estimation of inertial parameters of manipulator loads and links," *Int. J. Robotics Research,* vol. 5, pp. 101-119, Sep. 1986.

[7] H. Mayedda, K. Yoshida, and k. Osuka, "Base parameters of manipulator dynamic models," *IEEE Trans. Robot. Autom.,* vol. 6, pp. 312-321, Jun. 1990.

[8] M. Gautier and W. Khalil, "On the identification of the inertial parameters of robots," in *27th IEEE Conf. Decision and Control*, Austin, TX, 1988, pp. 2264-2269.

[9] M. W. Spong, S. Hutchinson, and M. Vidyasagar, *Robot Modeling and Control* 1ed. New Jersey: Wiley, 2005.

[10] W. Khalil, G. Gallot, and F. Boyer, "Dynamic modeling and simulation of a 3-D serial eel-like robot," *IEEE Trans. Syst. Man Cybern. C, Appl. Rev.,* vol. 37, pp. 1259-1268, Nov. 2007.

[11] B. Mooring, M. Driels, and Z. Roth, *Fundamentals of Manipulator Calibration*, 1 ed. New Jersey: Wiley, 1991.

[12] R. Y. Tsai and R. K. Lenz, "A new technique for fully autonomous and efficient 3D robotics hand/eye calibration," *IEEE Trans. Robot. Autom.,* vol. 5, pp. 345-358, Jun. 1989.

[13] J. Ghan and H. Kazerooni, "System identification for the Berkeley lower extremity exoskeleton (BLEEX)," in *IEEE Int. Conf. Robotics and Automation*, Orlando, FL, 2006, pp. 3477-3484

[14] J. Wu, J. Wanga, and Z. You, "An overview of dynamic parameter identification of robots," *Robotics and Computer-Integrated Manufacturing,* vol. 26, pp. 414-419, Oct. 2010.

[15] R. J. P. de Figueiredo, "A reproducing kernel Hilbert space (RKHS) approach to the optimal modeling, identification, and design of nonlinear adaptive systems," in *IEEE Adaptive Systems for Signal Processing, Communications, and Control Symp.*, Lake Louise, Alta., 2000, pp. 42-47.

[16] N.-T. Duy, B. Schoelkopf, and J. Peters, "Sparse online model learning for robot control with support vector regression," in *IEEE/RSJ Int. Conf. Intelligent Robots and Systems* St. Louis, MO, USA, 2009, pp. 3121-3126.

[17] N.-T. Duy and J. Peters, "Using model knowledge for learning inverse dynamics," in *IEEE Int. Conf. Robotics and Automation*, Anchorage, Alaska, USA, 2010, pp. 2677-2682

[18] H. A. Kingravi, G. Chowdhary, P. A. Vela, and E. N. Johnson, "Reproducing kernel Hilbert space approach for the online update of radial bases in neuro-adaptive control," *IEEE Trans. Neural Netw. Learn. Syst.,* vol. 23, pp. 1130-1141, Jul. 2012.

[19] F. Abdollahi, H. A. Talebi, and R. V. Patel, "Stable identification of nonlinear systems using neural networks: theory and experiments," *IEEE/ASME Trans. Mechatron.,* vol. 11, pp. 488-495, Aug. 2006.

[20] D. Kukolj and E. Levi, "Identification of complex systems based on neural and Takagi-Sugeno fuzzy model.," *IEEE Trans. Syst. Man Cybern. B, Cybern.,* vol. 34, pp. 2728-282, Feb. 2004.

[21] A. Yazdizadeh, K. Khorasani, and R. V. Patel, "Identification of a two-link flexible manipulator using adaptive time delay neural networks," *IEEE Trans. Syst. Man Cybern. B, Cybern.,* vol. 30, pp. 165-172, Feb. 2000.

[22] D. M. Katic and M. K. Vukobratovic, "Highly efficient robot dynamics learning by decomposed connectionist feedforward control structure," *IEEE Trans. Syst. Man Cybern. ,* vol. 25, pp. 145-158, Jan. 1995.

[23] G. Chowdhary, H. A. Kingravi, J. P. How, and P. A. Vela, "Bayesian nonparametric adaptive control using Gaussian processes," *IEEE Trans. Neural Netw. Learn. Syst.,* to be published, 2014.

[24] J. Ting, M. Mistry, J. Peters, S. Schaal, and J. Nakanishi, "A Bayesian Approach to Nonlinear Parameter Identification for Rigid Body Dynamics," in *Robotics: Science and Systems*, Philadelphia, USA, 2006.

[25] Z.-H. Jiang, T. Ishida, and M. Sunawada, "Neural network aided dynamic parameter identification of robot manipulators," in *IEEE Int. Conf. Syst., Man, and Cybern.*, Taipei, 2006, pp. 3298-3303.

[26] C. C. Cheah, C. Liu, and J. J. E. Slotine, "Adaptive jacobian tracking control of robots with uncertainties in kinematic, dynamic and actuator models," *IEEE Trans. Automat. Control,* vol. 51, pp. 1024-1029, Jun. 2005.

[27] M. Ahmadipour, A. Khayatian, and M. Dehghani, "Adaptive backstepping control of rigid-link electrically driven robots with uncertain kinematics and dynamics," in *2nd Int. Conf. Control, Instrumentation and Automation*, Shiraz, 2011, pp. 911-916.

[28] H.-S. Ahn, Y. Q. C. Chen, and K. L. Moore, "Iterative learning control: brief survey and categorization," *IEEE Trans. Syst. Man Cybern. C, Appl. Rev.,* vol. 37, pp. 1099-1121, Nov. 2007.

[29] C.-A. Cheng , H.-P. Huang, H.-K. Hsu , W.-Z. Lai , C.-C. Cheng , and Y.-C. Li "Identification of the inverse dynamics of robot manipulators with the structured kernel," in *CACS Int. Automatic Control Conf.*, Nantou, Taiwan, 2013, pp. 266-271.

[30] B. Siciliano and O. Khatib, *Springer Handbook of Robotics*. New York: Springer, 2008.

[31] B. Schoelkopf and A. J. Smola, *Learning with Kernels*. Cambridge, MA: The MIT Press, 2001.

[32] N. Aronszajn, "Theory of reproducing kernels," *Trans. Amer. Math. Soc.,* vol. 68, pp. 337-404, May 1950.

[33] F. Cucker and D. X. Zhou, *Learning Theory - An Approximation Theory Viewpoint*. New York: Cambridge University Press, 2007.

[34] F. Cucker and S. Smale, "On the mathematical foundations of learning," *Bulletin Amer. Math. Soc.,* vol. 39, pp. 1-49, Nov. 2002.

[35] C. Bergmeir and J. M. Benitez, "On the use of cross-validation for time series predictor evaluation," *Inform. Sci.,* vol. 191, pp. 192-213, May 2012.

[36] P. K. Khosla and T. Kanade, "Experimental evaluation of nonlinear feedback and feedforward control schemes for manipulators," *Int. J. Robotics Research,* vol. 7, pp. 18-28, Feb. 1988.

Ching-An Cheng received double B.S. degrees in mechanical engineering and electrical engineering from National Taiwan University, Taipei, Taiwan, in 2011, and the M.S. degree in mechanical engineering from National Taiwan University in 2013. Currently, he is pursuing the Ph.D. degree in robotics at Georgia Institute of Technology.

From 2014 to 2015, he was a research assistant at NTU Robotics Laboratory, Department of Mechanical Engineering, National Taiwan University. His research has been concerned with robot control and learning, reproducing kernel Hilbert space, system dynamics and identification, human-robot interaction, and exoskeletons.

Han-Pang Huang (S'83–M'86) received the M.S. and the Ph.D. degrees in electrical engineering from The University of Michigan, Ann Arbor in 1982 and 1986, respectively.

Since 1986, he has been with National Taiwan University, Taipei, Taiwan, where he is currently a professor in the Department of Mechanical Engineering and the Graduate Institute of Industrial Engineering and serves as the Director of NTU Robotics Laboratory. He has been elected as a Distinguished Professor of the National Taiwan University since August 2006, and has held the position of Zhong Zhuo-Zhang Chair Professor since 2009. He served as the Director of Manufacturing Automation Technology Research Center, Associate Dean of the College of Engineering, the Director of the Graduate Institute of Industrial Engineering, and the Chairperson of Mechanical Engineering, all in National Taiwan University. His research interests include machine intelligence, humanoid robots, intelligent robotic systems, prosthetic hands, nanomanipulation, and nonlinear systems.

Prof. Huang was the Editor-in-Chief of the Journal of Chinese Fuzzy System Association (1997-1999), the Editor-in-Chief of the International Journal of Fuzzy System (1999-2002), the Associate Editor of IEEE Trans. on Automation Science and Engineering (2003- 2005), and the Editorial Board Member of International Journal of Advanced Robotics (2004-2008), Intl. J. of Service Robots, the Associate Editor of International Journal of Advanced Robotics Systems, the Associate Editor of IEEE/ASME Trans. on Mechatronics, and the Publication Management Committee of IEEE/ASME journals. Currently, he is on the Editorial board of the International Journal of Electronic Business Management, and the Editor of the Intl. J. of Automation and Smart Technology. He received the Ford University Research Award (1996-1998). He has received three-time Distinguished Research Awards (1996—2002), twice Research Fellow Awards (2002-2008), and Distinguished Research Fellow Awards (2009) from National Science Council, Taiwan R.O.C. He received the Distinguished Education Award on RFID from EPCglobal (2010), TECO Outstanding Science and Technology Research Achievement Award (2012), HIWIN Distinguished Industry Creation Award (2014). He was awarded the Fellow of CIAE (Chinese Institute of Automation Engineers, 2010), the Fellow of CSME (Chinese Society of Mechanical Engineers, 2011). He was named in Who's Who in the World 2001, 2002, and Who's Who in the R.O.C. 2002. He has served as committee chairs/co-chairs, members in many national, international, and IEEE conferences.

Huan-Kun Hsu received the B.S. and the M.S. degrees from National Chiao Tung University, Hsinchu, Taiwan, in 2006 and 2008, respectively.

During 2010–2011, he was a researcher at Taiwan Shin Kong Security company. From 2011 to now, he has been a Ph.D. student at NTU Robotics Laboratory, Department of Mechanical Engineering, National Taiwan University, Taipei, Taiwan. His current research interests include bipedal walking and humanoid robots.

Wei-Zh Lai received the B.S. and the M.S. degrees in mechanical engineering from National Taiwan University, Taipei, Taiwan, in 2012 and 2014, respectively.

Since 2014, he has been a researcher with Syntec Ltd., Hsinchu, Taiwan. His research focuses on legged robots and motion control.

Chih-Chun Cheng received the B.S. and the M.S. degrees in mechanical engineering from National Taiwan University, Taipei, Taiwan, in 2012 and 2014. His current research interests include anthropomorphic robot hand and grasping.